Results from the first use of low radioactivity argon in a dark matter search

P. Agnes,[1] L. Agostino,[2] I. F. M. Albuquerque,[3,4] T. Alexander,[5,6] A. K. Alton,[7] K. Arisaka,[8] H. O. Back,[3,9] B. Baldin,[6] K. Biery,[6] G. Bonfini,[10] M. Bossa,[11,10] B. Bottino,[12,13] A. Brigatti,[14] J. Brodsky,[3] F. Budano,[15,16] S. Bussino,[15,16] M. Cadeddu,[17,18] L. Cadonati,[5] M. Cadoni,[17,18] F. Calaprice,[3] N. Canci,[19,10] A. Candela,[10] H. Cao,[3] M. Cariello,[13] M. Carlini,[10] S. Catalanotti,[20,21] P. Cavalcante,[22,10] A. Chepurnov,[23] A. G. Cocco,[21] G. Covone,[20,21] L. Crippa,[24,14] D. D'Angelo,[24,14] M. D'Incecco,[10] S. Davini,[11,10] S. De Cecco,[2] M. De Deo,[10] M. De Vincenzi,[15,16] A. Derbin,[25] A. Devoto,[17,18] F. Di Eusanio,[3] G. Di Pietro,[10,14] E. Edkins,[26] A. Empl,[19] A. Fan,[8] G. Fiorillo,[20,21] K. Fomenko,[27] G. Forster,[5,6] D. Franco,[1] F. Gabriele,[10] C. Galbiati,[3,14] C. Giganti,[2] A. M. Goretti,[10] F. Granato,[20,28] L. Grandi,[29] M. Gromov,[23] M. Guan,[30] Y. Guardincerri,[6,29] B. R. Hackett,[26] J. Hall,[31] K. Herner,[6] P. H. Humble,[31] E. V. Hungerford,[19] Al. Ianni,[32,10] An. Ianni,[3,10] I. James,[15,16] C. Jollet,[33] K. Keeter,[34] C. L. Kendziora,[6] V. Kobychev,[35] G. Koh,[3] D. Korablev,[27] G. Korga,[19,10] A. Kubankin,[36] X. Li,[3] M. Lissia,[18] P. Lombardi,[14] S. Luitz,[37] Y. Ma,[30] I. N. Machulin,[38,39] A. Mandarano,[11,10] S. M. Mari,[15,16] J. Maricic,[26] L. Marini,[12,13] C. J. Martoff,[28,*] A. Meregaglia,[33] P. D. Meyers,[3] T. Miletic,[28] R. Milincic,[26] D. Montanari,[6] A. Monte,[5] M. Montuschi,[10] M. Monzani,[37] P. Mosteiro,[3] B. J. Mount,[34] V. N. Muratova,[25] P. Musico,[13] J. Napolitano,[28] A. Nelson,[3] S. Odrowski,[10] M. Orsini,[10] F. Ortica,[40,41] L. Pagani,[12,13] M. Pallavicini,[12,13] E. Pantic,[42,†] S. Parmeggiano,[14] K. Pelczar,[43] N. Pelliccia,[40,41] S. Perasso,[1] A. Pocar,[5,3] S. Pordes,[6] D. A. Pugachev,[38,39] H. Qian,[3] K. Randle,[5] G. Ranucci,[14] A. Razeto,[10,3] B. Reinhold,[26] A. L. Renshaw,[8,19] A. Romani,[40,41] B. Rossi,[21,3] N. Rossi,[10] D. Rountree,[22] D. Sablone,[10] P. Saggese,[14] R. Saldanha,[29] W. Sands,[3] S. Sangiorgio,[44] C. Savarese,[11,10] E. Segreto,[45] D. A. Semenov,[25] E. Shields,[3] P. N. Singh,[19] M. D. Skorokhvatov,[38,39] O. Smirnov,[27] A. Sotnikov,[27] C. Stanford,[3] Y. Suvorov,[8,10,38] R. Tartaglia,[10] J. Tatarowicz,[28] G. Testera,[13] A. Tonazzo,[1] P. Trinchese,[20] E. V. Unzhakov,[25] A. Vishneva,[27] B. Vogelaar,[22] M. Wada,[3] S. Walker,[20,21] H. Wang,[8] Y. Wang,[30,8,46] A. W. Watson,[28] S. Westerdale,[3] J. Wilhelmi,[28] M. M. Wojcik,[43] X. Xiang,[3] J. Xu,[3] C. Yang,[30] J. Yoo,[6] S. Zavatarelli,[13] A. Zec,[5] W. Zhong,[30] C. Zhu,[3] and G. Zuzel[43]

(DarkSide Collaboration)

[1]*APC, Université Paris Diderot, CNRS/IN2P3, CEA/Irfu, Obs. de Paris, Sorbonne Paris Cité, Paris 75205, France*
[2]*LPNHE Paris, Université Pierre et Marie Curie, Université Paris Diderot, CNRS/IN2P3, Paris 75252, France*
[3]*Department of Physics, Princeton University, Princeton, New Jersey 08544, USA*
[4]*Instituto de Física, Universidade de São Paulo, São Paulo 05508-090, Brazil*
[5]*Amherst Center for Fundamental Interactions and Department of Physics, University of Massachusetts, Amherst, Massachusetts 01003, USA*
[6]*Fermi National Accelerator Laboratory, Batavia, Illinois 60510, USA*
[7]*Department of Physics, Augustana University, Sioux Falls, South Dakota 57197, USA*
[8]*Department of Physics and Astronomy, University of California, Los Angeles, California 90095, USA*
[9]*Pacific Northwest National Laboratory, Richland, Washington 99354, USA*
[10]*Laboratori Nazionali del Gran Sasso, Assergi AQ 67010, Italy*
[11]*Gran Sasso Science Institute, L'Aquila AQ 67100, Italy*
[12]*Department of Physics, Università degli Studi, Genova 16146, Italy*
[13]*Istituto Nazionale di Fisica Nucleare, Sezione di Genova, Genova 16146, Italy*
[14]*Istituto Nazionale di Fisica Nucleare, Sezione di Milano, Milano 20133, Italy*
[15]*Istituto Nazionale di Fisica Nucleare, Sezione di Roma Tre, Roma 00146, Italy*
[16]*Department of Physics and Mathematics, Università degli Studi Roma Tre, Roma 00146, Italy*
[17]*Department of Physics, Università degli Studi, Cagliari 09042, Italy*
[18]*Istituto Nazionale di Fisica Nucleare, Sezione di Cagliari, Cagliari 09042, Italy*
[19]*Department of Physics, University of Houston, Houston, Texas 77204, USA*
[20]*Department of Physics, Università degli Studi Federico II, Napoli 80126, Italy*
[21]*Istituto Nazionale di Fisica Nucleare, Sezione di Napoli, Napoli 80126, Italy*
[22]*Department of Physics, Virginia Tech, Blacksburg, Virginia 24061, USA*
[23]*Skobeltsyn Institute of Nuclear Physics, Lomonosov Moscow State University, Moscow 119991, Russia*
[24]*Department of Physics, Università degli Studi, Milano 20133, Italy*
[25]*St. Petersburg Nuclear Physics Institute NRC Kurchatov Institute, Gatchina 188350, Russia*
[26]*Department of Physics and Astronomy, University of Hawai'i, Honolulu, Hawaii 96822, USA*
[27]*Joint Institute for Nuclear Research, Dubna 141980, Russia*
[28]*Department of Physics, Temple University, Philadelphia, Pennsylvania 19122, USA*
[29]*Kavli Institute, Enrico Fermi Institute, and Dept. of Physics, University of Chicago, Chicago, Illinois 60637, USA*
[30]*Institute of High Energy Physics, Beijing 100049, China*

[31]*Pacific Northwest National Laboratory, Richland, Washington 99352, USA*
[32]*Laboratorio Subterráneo de Canfranc, Canfranc Estación 22880, Spain*
[33]*IPHC, Université de Strasbourg, CNRS/IN2P3, Strasbourg 67037, France*
[34]*School of Natural Sciences, Black Hills State University, Spearfish, South Dakota 57799, USA*
[35]*Institute for Nuclear Research, National Academy of Sciences of Ukraine, Kiev 03680, Ukraine*
[36]*Radiation Physics Laboratory, Belgorod National Research University, Belgorod 308007, Russia*
[37]*SLAC National Accelerator Laboratory, Menlo Park, California 94025, USA*
[38]*National Research Centre Kurchatov Institute, Moscow 123182, Russia*
[39]*National Research Nuclear University MEPhI, Moscow 115409, Russia*
[40]*Department of Chemistry, Biology and Biotechnology, Università degli Studi, Perugia 06123, Italy*
[41]*Istituto Nazionale di Fisica Nucleare, Sezione di Perugia, Perugia 06123, Italy*
[42]*Department of Physics, University of California, Davis, California 95616, USA*
[43]*Smoluchowski Institute of Physics, Jagiellonian University, Krakow 30348, Poland*
[44]*Lawrence Livermore National Laboratory, Livermore, California 94550, USA*
[45]*Institute of Physics Gleb Wataghin, Universidade Estadual de Campinas, São Paulo 13083-859, Brazil*
[46]*School of Physics, University of Chinese Academy of Sciences, Beijing 100049, China*

Liquid argon is a bright scintillator with potent particle identification properties, making it an attractive target for direct-detection dark matter searches. The DarkSide-50 dark matter search here reports the first WIMP search results obtained using a target of low-radioactivity argon. DarkSide-50 is a dark matter detector, using a two-phase liquid argon time projection chamber, located at the Laboratori Nazionali del Gran Sasso. The underground argon is shown to contain ^{39}Ar at a level reduced by a factor $(1.4 \pm 0.2) \times 10^3$ relative to atmospheric argon. We report a background-free null result from (2616 ± 43) kg d of data, accumulated over 70.9 live days. When combined with our previous search using an atmospheric argon, the 90% C.L. upper limit on the WIMP-nucleon spin-independent cross section, based on zero events found in the WIMP search regions, is 2.0×10^{-44} cm^2 (8.6×10^{-44} cm^2, 8.0×10^{-43} cm^2) for a WIMP mass of 100 GeV/c^2 (1 TeV/c^2, 10 TeV/c^2).

The existence of dark matter in the Universe is inferred from abundant astrophysical and cosmological observations [1–3]. The DarkSide-50 experiment searches for dark matter in the form of weakly interacting massive particles (WIMPs) [4], whose collisions with argon nuclei would produce nuclear recoils (NRs) with tens of keV energy. Liquid argon (LAr) is a bright scintillator and allows for efficient drift and extraction of the ionization electrons. Pulse shape discrimination (PSD) in LAr allows electron recoil (ER) events from β-γ backgrounds to be rejected relative to the NR events expected from WIMP scattering at the 1.5×10^7 level or better [5,6]. However, atmospheric argon (AAr) contains ~1 Bq/kg of cosmic-ray-produced ^{39}Ar activity [7,8]. A source of argon with reduced ^{39}Ar activity is a crucial requirement for developing experiments that will push argon-based WIMP dark matter direct detection searches to their highest possible sensitivity. This report presents the first results from a direct-detection WIMP dark matter search using a target of low-radioactivity argon (UAr), which was extracted and purified in a multi-year effort [9–12].

The DarkSide-50 two-phase (liquid-gas) argon time projection chamber (LAr TPC) is mounted at the center of a liquid scintillator veto (LSV) described in Ref. [13].

The LSV is instrumented with 110 PMTs and filled with 30 t of boron-loaded liquid scintillator. Surrounding the LSV is a 1 kt water Cerenkov veto (WCV) instrumented with 80 PMTs. Signals from the LSV and WCV are used to reject events in the LAr TPC caused by cosmic-ray muons [14,15], cosmogenic (muon-induced) neutrons [16,17] or radiogenic neutrons and γ rays from radioactive contamination in the detector components.

The LAr TPC is fully described in Ref. [6]. A total of 38 3" PMTs, 19 positioned at the top and 19 at the bottom of a (46.4 ± 0.7) kg active target of UAr, detect primary scintillation (S1) and gas scintillation from drifted ionization electrons (S2) resulting from ionizing radiation interactions. The TPC drift field is 200 V/cm and the extraction field is 2.8 kV/cm. PSD of ER events is based on the single parameter f$_{90}$, the fraction of S1 light detected in the first 90 ns of the pulse. The S1 and S2 signals together enable three-dimensional event localization. The transverse (x-y) position is determined from the hit pattern of the S2 signal on the top PMT array, while the vertical (z) position is inferred from the drift time separating the S1 and S2 signals. The S1 response is corrected for z dependence, and the S2 response is corrected for radial dependence, normalizing both to the respective centers of the detector. Other spatial dependencies are not significant (S1 radial dependence is <3%, S2 z dependence is consistent with an electron drift lifetime >5 ms). The fully corrected

*jeff.martoff@temple.edu
†pantic@ucdavis.edu

zero-field TPC photoelectron yield with UAr at the ^{83m}Kr peak energy is (8.1 ± 0.2) PE/keV, 2% higher than that quoted in Ref. [6], due to small changes in the baseline finding and pulse identification algorithms.

Figure 1 compares the UAr and AAr data of the S1 pulse integral spectrum. A z cut (residual mass of ∼34 kg) has been applied to remove γ-ray events from the anode and cathode windows. Events identified as multiple scatters or coincident with a prompt signal in the LSV have also been removed. To compare the ER background from UAr with that from AAr, a GEANT4 [18,19] MC simulation of the DarkSide-50 LAr TPC, LSV, and WCV detectors was developed. The simulation accounts for material properties, optics, and readout noise and also includes a model for LAr scintillation and recombination. The MC is tuned to agree with the high statistics ^{39}Ar data taken with AAr [6]. A simultaneous MC fit to the S1 spectrum taken with field off (see Fig. 6 in Appendix A), S1 spectrum with field on, and the z-position distribution of events, determines the ^{39}Ar and ^{85}Kr activities in the UAr to be (0.73 ± 0.11) mBq/kg and (2.05 ± 0.13) mBq/kg, respectively. The fitted ^{39}Ar and ^{85}Kr activities are also shown in Fig. 1. The uncertainties in the fitted activities are dominated by systematic uncertainties from varying fit conditions. The ^{39}Ar activity of the UAr corresponds to a reduction by a factor of $(1.4 \pm 0.2) \times 10^3$ relative to AAr. This is significantly beyond the upper limit of 150 established in [12].

An independent estimate of the ^{85}Kr decay rate in UAr is obtained by identifying β-γ coincidences from the 0.43% decay branch to metastable ^{85m}Rb with mean lifetime 1.46 μs. This method gives a decay rate of ^{85}Kr via ^{85m}Rb of (33.1 ± 0.9) events/d in agreement with the value (35.3 ± 2.2) events/d obtained from the known branching ratio and the spectral fit result. The presence

of ^{85}Kr in UAr is unexpected. We have not attempted to remove krypton from the UAr, although cryogenic distillation would likely do this very effectively. The ^{85}Kr in UAr could come from atmospheric leaks or from natural fission underground, which produces ^{85}Kr in deep underground water reservoirs at specific activities similar to those of ^{39}Ar [20].

As in Ref. [6], we determine the nuclear recoil energy scale from the S1 signal using the photoelectron yield of NRs relative to ^{83m}Kr measured in the SCENE experiment [21,22], and the zero-field photoelectron yield for ^{83m}Kr measured in DarkSide-50. An *in situ* calibration with an AmBe source was also performed, allowing a check of the f_{90} medians obtained for NRs in DarkSide-50 with those scaled from SCENE, as shown in Fig. 2. Contamination from inelastic or coincident electromagnetic scattering cannot easily be removed from AmBe calibrations, so we still derive our NR acceptance from SCENE data where available.

High-performance neutron vetoes are necessary to exclude NR events due to radiogenic or cosmic-ray-produced neutrons from the WIMP search. In the AAr exposure [6], the vetoing efficiency of the LSV was limited to $98.5 \pm 0.5\%$ by dead-time considerations given the ∼150 kBq of ^{14}C in the scintillator, resulting from the unintended use of trimethylborate (TMB). For the UAr data set, the LSV contains a scintillator mixture of low-radioactivity TMB from a different supplier at 5% concentration by mass. As a result, the ^{14}C activity in the LSV scintillator is now only ∼0.3 kBq.

Neutron capture on ^{10}B in the scintillator occurs with a 22 μs lifetime through two channels [13,23]:
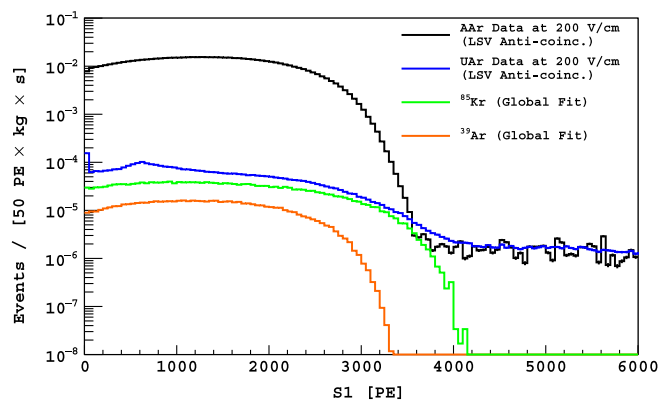

FIG. 1. Live-time normalized S1 pulse integral spectra from single-scatter events in AAr (black) and UAr (blue) taken with 200 V/cm drift field. Also shown are the ^{85}Kr (green) and ^{39}Ar (orange) levels as inferred from a MC fit. Note the peak in the lowest bin of the UAr spectrum, which is due to ^{37}Ar from cosmic-ray activation. The peak at ∼600 PE is due to γ-ray Compton backscatters.
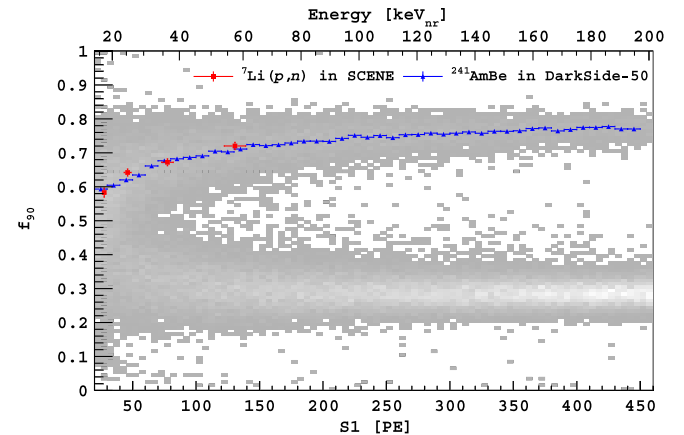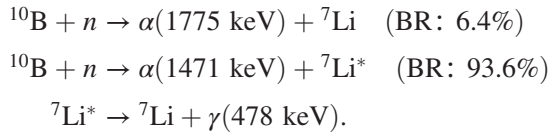

FIG. 2. f_{90} NR median vs S1 from a high-rate *in situ* AmBe calibration (blue) and scaled from SCENE measurements (red points). Grey points indicate the upper NR band from the AmBe calibration and lower ER band from β-γ backgrounds. Events in the region between the NR and ER bands are due to inelastic scattering of high-energy neutrons, accidentals, and correlated neutron and γ-ray emission by the AmBe source.

$$^{10}\text{B} + n \rightarrow \alpha(1775 \text{ keV}) + {}^{7}\text{Li} \quad (\text{BR: } 6.4\%)$$

$$^{10}\text{B} + n \rightarrow \alpha(1471 \text{ keV}) + {}^{7}\text{Li}^* \quad (\text{BR: } 93.6\%)$$

$$^{7}\text{Li}^* \rightarrow {}^{7}\text{Li} + \gamma(478 \text{ keV}).$$

The reduced radioactivity of the LSV scintillator allowed us to operate with a veto window of 6 times the neutron capture lifetime and a threshold low enough to veto on the signal from the α and ^{7}Li (g.s) capture channel. Using AmBe calibration data, we measured that this signal is quenched to 30 ± 5 PE, well above our analysis threshold of 6 PE. The 478 keV γ ray accompanying the ^{7}Li* channel gives at least 240 PE and is easily detected. From AmBe data and MC simulations, we estimate a detection efficiency of $> 99.1\%$ [13] for radiogenic neutrons when using the neutron capture signals only. This estimate is a lower limit since the calculation neglects the neutron thermalization signal from the scintillator. The main detection inefficiency is due to the fraction of the neutron captures on ^{1}H in which the 2.2 MeV deexcitation γ ray is fully absorbed in inert materials rather than in the scintillator.

The data for the WIMP search were acquired using a simple majority trigger requiring a threshold number of channels in the LAr TPC to present hits within a 100 ns window. The trigger efficiency is essentially 100% for NRs in our WIMP search region. We perform a nonblind physics analysis, where the LAr TPC event selection and data analysis procedures are intentionally kept as similar as possible to those used in the AAr exposure [6]. After data quality cuts, we obtain 70.9 live days of WIMP search data with the UAr.

Events are further required to have only one valid and unsaturated S1, one valid S2 pulse with position-corrected value greater than 100 PE, and up to one "S3" pulse, due to S2-induced photoionization of the cathode. A pulse is identified as S3 if the time difference between S2 and the pulse matches the maximum drift time. Additionally, we remove events in which the S1 light is abnormally concentrated in a single PMT, which could be due to an afterpulse or to a Cherenkov interaction in a PMT window piled up with a normal S1 pulse. The much lower ^{39}Ar rate in UAr revealed a higher fraction of spurious events, leading us to adjust the cut to reject 5% of events rather than 1% as in the AAr run.

The remaining events are subject to being vetoed as neutron-associated. Events are vetoed if the LSV detected a prompt signal near the LAr TPC trigger time or if the LSV detected a delayed signal above 3 PE within 200 μs after a TPC interaction (delayed neutron captures). Events with LSV activity preceding the LAr TPC signal by up to $\sim 8 \ \mu$s are also vetoed to account for possible delayed neutron events in the TPC. Finally, all LAr TPC events are rejected for 2 s after a TPC trigger in coincidence with any large-amplitude muonlike event in the WCV or LSV to eliminate delayed neutrons possibly produced by the muon.

With the same z cuts in the TPC as in Ref. [6], a fiducial mass of (36.9 ± 0.6) kg remains. No x-y cut is applied

because the PSD, z cut and veto cuts are more than adequate to remove the γ-ray background strongly concentrated at the boundaries of the sensitive volume. Surface backgrounds from α emitters of the natural radioactive decay chains have been identified and studied, but none of these survive the standard cuts to give background in the WIMP search region at the present background and exposure levels.

The combined acceptance of all TPC and veto cuts to retain single-scatter NR events is shown as a function of S1 in Fig. 3. The acceptance is $> 70\%$ and approximately independent of S1 above 20 PE, with the major loss being due to the dead time from the delayed neutron capture veto cut. The distribution of the 1.26×10^5 events in the f_{90} vs S1 plane which remain after all cuts is shown in Fig. 4.

As was done for the AAr exposure, the WIMP search region is defined as a region in the f_{90} vs S1 plane having known high acceptance for NRs and low expected leakage of single-scatter ER events, with an energy region of interest of 20 PE to 460 PE in S1 (13 keV$_{\text{nr}}$ to 201 keV$_{\text{nr}}$). NR acceptance curves are established using the median f_{90} values for NRs measured in the SCENE experiment [21,22], inserted into a statistical model for the f_{90} distribution, as described in Refs. [5,6,24]. Above 57 keV$_{\text{nr}}$, where SCENE data are unavailable, the NR f_{90} medians are taken from DarkSide-50 AmBe calibration data (see Fig. 2).

The expected single-scatter ER leakage is calculated from the same statistical model for the ER f_{90} distribution as described in Ref. [6], fitted to the high statistics ^{39}Ar data from the AAr exposure, and scaled to the number of events in the UAr data sample. The WIMP search region is then defined by intersecting the 90% NR acceptance line with the curve corresponding to a leakage of less than 0.01 events/(5-PE bin) from the single-scatter ER background into the WIMP search region. This procedure predicts a total of less than 0.1 leakage events. As can be seen in Fig. 4, there are in fact no events in the WIMP search region in the present UAr exposure.
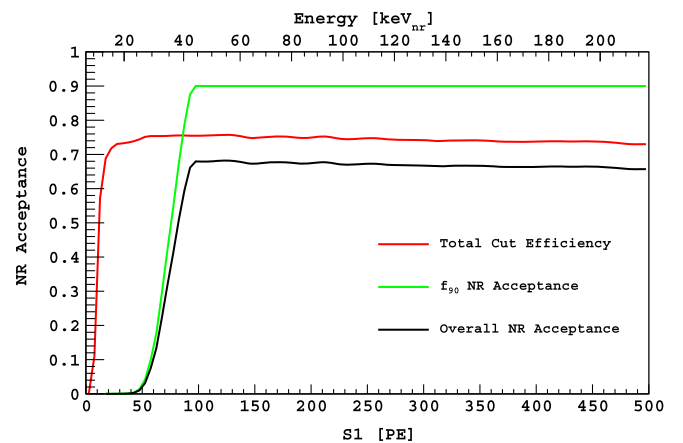

FIG. 3. Combined acceptance of all TPC and veto cuts (red), acceptance of the f_{90} NR cut (green) and the final cumulative NR acceptance in UAr data (black).
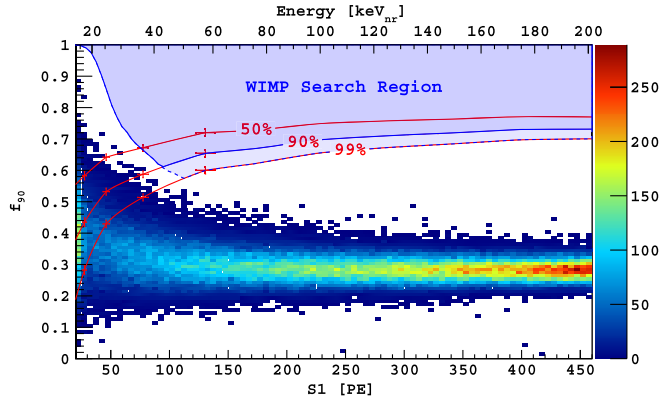
FIG. 4.   Distribution of events in the f_{90} vs S1 plane surviving all cuts in the energy region of interest. Shaded blue with solid blue outline: WIMP search region. The red points (with their uncertainties) are derived from the SCENE measurements of NR acceptance. The f_{90} acceptance contours are drawn by connecting the red points and extending the contours using DarkSide-50 AmBe data (see text). Lighter shaded blue with dashed blue line show that extending the WIMP search region to 99% f_{90} NR acceptance is still far from ER backgrounds.

We can compare the observed number of "neutron events"—events within the WIMP search region that pass the TPC cuts and are accompanied by veto signals—with our MC prediction. We do not observe any neutron events in the present exposure. In the previous AAr exposure of 47.1 live days [6] we observed two. One of the AAr neutron events was classified as cosmogenic based on its WCV and LSV signals. Combining the two exposures, we observe one radiogenic neutron event in 118 live days of data, which is in agreement with our MC prediction of (2 ± 2) events before the veto cuts. MC simulations for the UAr exposure predict that <0.02 radiogenic neutrons would produce events in the TPC and remain un-vetoed. The unvetoed cosmogenic neutron background is expected to be small compared to the radiogenic neutron background [17].

Dark matter limits from the present exposure are determined from our WIMP search region using the standard isothermal galactic WIMP halo parameters ($v_{escape} = 544$ km/s, $v_0 = 220$ km/s, $v_{Earth} = 232$ km/s, $\rho_{dm} = 0.3$ GeV/$(c^2 cm^3)$; see [6] and references cited therein). Given the background-free result shown above, we derive a 90% C.L. exclusion curve corresponding to the observation of 2.3 events for spin-independent interactions. The null result of the UAr exposure sets the upper limit on the WIMP-nucleon spin-independent cross section of 3.1×10^{-44} cm^2 (1.4×10^{-43} cm^2, 1.3×10^{-42} cm^2) for a WIMP mass of 100 GeV/c^2 (1 TeV/c^2, 10 TeV/c^2). When combined [25] with the null result of our previous AAr exposure, we obtain an upper limit of 2.0×10^{-44} cm^2 (8.6×10^{-44} cm^2, 8.0×10^{-43} cm^2) for a WIMP mass of 100 GeV/c^2 (1 TeV/c^2, 10 TeV/c^2). Figure 5 compares these limits to those obtained by other experiments.
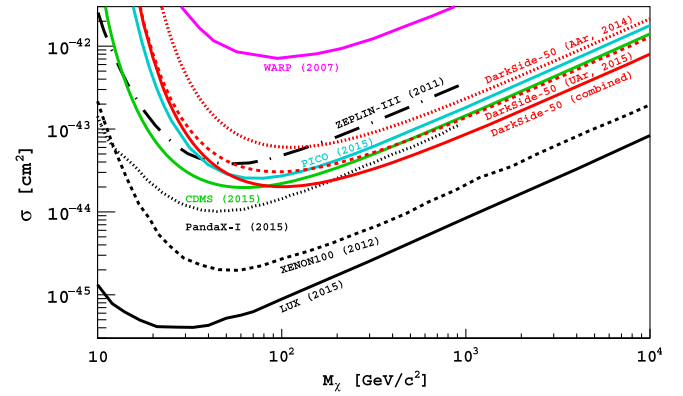

FIG.   5.   Spin-independent   WIMP-nucleon   cross   section 90% C.L. exclusion plots for the DarkSide-50 AAr (dotted red) and UAr campaigns (dashed red), and combination of the UAr and AAr [6] campaigns (solid red). Also shown are results from LUX [26](solid black), XENON100 [27] (dashed black), PandaX-I [28] (dotted black), CDMS [29] (solid green), PICO [30] (solid cyan), ZEPLIN-III [31] (dash dotted black) and WARP [32] (magenta).

The DarkSide-50 detector is currently accumulating exposure in a stable, low-background configuration with the characteristics described above. We plan to conduct a 3-yr dark matter search with increased calibration statistics and several improvements in data analysis (see Fig. 7 in Appendix A). These first results show that UAr can significantly extend the potential of argon for WIMP dark matter searches. The ER rejection previously demonstrated in AAr data and the reduction of ^{39}Ar shown here already imply that UAr exposures of at least 5.5 tonne-yr can be made free of ^{39}Ar background.
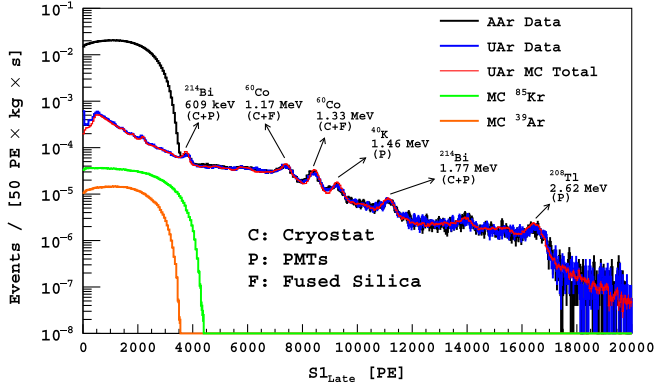
FIG. 6. Comparison of the measured field off spectra for the UAr (blue) and AAr (black) targets, normalized to exposure. Also shown are the MC fit to the UAr data (red) and individual components of ^{85}Kr (green) and ^{39}Ar (orange) extracted from the fit.

APPENDIX: FIELD OFF SPECTRA AND S2/S1 CUT

Figure 6 compares the measured field off spectra for the UAr (blue) and AAr (black) targets, normalized to exposure. The horizontal axis ("S1-late") is the integral of the S1 pulse from 90 ns to 7 μs, which includes $\sim$70% of the total S1 light for electron recoils (ERs). Despite the sacrifice of photoelectron statistics, use of S1-late avoids distortion of the spectra by digitizer saturation at high S1 values (S1 $> 2 \times 10^3$ PE) and, with the asymmetry correction for S1 described above, gives a net improvement in the pulse height resolution. The background γ-ray lines originate from identified levels of ^{238}U, ^{232}Th, ^{40}K, and ^{60}Co in the detector construction materials and are consistent with the expectations from our materials screening. The
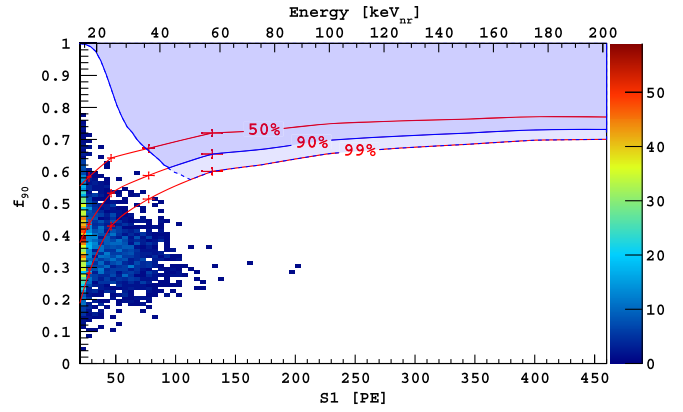

FIG. 7. Distribution of events in the f_{90} vs S1 plane which survive all quality and physics cuts (including veto cuts), and which in addition survive a radial cut and a S2/S1 cut. Shaded blue with solid blue outline: WIMP search region. Lighter shaded blue with dashed blue line show that extending the WIMP search region to 99% f_{90} NR acceptance is still far away from ER backgrounds.

repeatability in the positions of the peaks in the AAr and UAr data shows the stability of the detector system as a whole.

Figure 7 demonstrates available improvements in background rejection, which we do not utilize in this analysis. When adding an S2/S1 cut (requiring that S2/S1 be lower than the median value for NRs) and also xy fiducialization (requiring the reconstructed radius to be less than 10 cm), we obtain an even greater separation between the events surviving the selection and the previously defined WIMP search region. Should a signal appear in the region of interest, the S2/S1 parameter would provide a powerful additional handle in understanding its origin.

[1] S. M. Faber and J. S. Gallagher, Annu. Rev. Astron. Astrophys. **17**, 135 (1979).

[2] D. N. Spergel, Phys. Rev. D **37**, 1353 (1988).

[3] D. Clowe, M. Bradač, A. H. Gonzalez, M. Markevitch, S. W. Randall, C. Jones, and D. Zaritsky, Astrophys. J. **648**, L109 (2006).

[4] J. L. Feng, Annu. Rev. Astron. Astrophys. **48**, 495 (2010).

[5] M. G. Boulay and A. Hime, Astropart. Phys. **25**, 179 (2006).

[6] P. Agnes *et al.* (The DarkSide Collaboration), Phys. Lett. B **743**, 456 (2015).

[7] H. H. Loosli, Earth Planet. Sci. Lett. **63**, 51 (1983).

[8] P. Benetti *et al.* (The WArP Collaboration), Nucl. Instrum. Methods Phys. Res., Sect. A **574**, 83 (2007).

[9] D. Acosta-Kane *et al.*, Nucl. Instrum. Methods Phys. Res., Sect. A **587**, 46 (2008).

[10] H. O. Back *et al.*, arXiv:1204.6024v2.

[11] H. O. Back *et al.*, arXiv:1204.6061v2.

[12] J. Xu *et al.*, Astropart. Phys. **66**, 53 (2015).

[13] P. Agnes *et al.* (The DarkSide Collaboration), J. Instrum. **11**, P03016 (2016).

[14] G. Bellini *et al.* (The Borexino Collaboration), J. Instrum. **6**, P05005 (2011).

[15] G. Bellini *et al.* (The Borexino Collaboration), J. Cosmol. Astropart. Phys. 05 (2012) 015.

[16] G. Bellini *et al.* (The Borexino Collaboration), J. Cosmol. Astropart. Phys. 08 (2013) 049.

[17] A. Empl, E. V. Hungerford, R. Jasim, and P. Mosteiro, J. Cosmol. Astropart. Phys. 08 (2014) 064.

[18] S. Agostinelli *et al.*, Nucl. Instrum Methods Phys. Res., Sect. A **506**, 250 (2003).

[19] J. Allison *et al.*, IEEE Trans. Nucl. Sci. **53**, 270 (2006).

[20] B. E. Lehmann, S. N. Davis, and J. T. Fabryka-Martin, Water Resour. Res. **29**, 2027 (1993).

[21] T. Alexander *et al.* (The SCENE Collaboration), Phys. Rev. D **88**, 092006 (2013).

[22] H. Cao *et al.* (The SCENE Collaboration), Phys. Rev. D **91**, 092007 (2015).

[23] A. Wright, P. Mosteiro, B. Loer, and F. P. Calaprice, Nucl. Instrum. Methods Phys. Res., Sect A **644**, 18 (2011).

[24] D. V. Hinkley, Biometrika **56**, 635 (1969).

[25] S. Yellin, arXiv:1105.2928.

[26] D. S. Akerib *et al.* (The LUX Collaboration), arXiv:1512.03506v1.

[27] E. Aprile *et al.* (The XENON100 Collaboration), Phys. Rev. Lett. **109**, 181301 (2012).

[28] X. Xiao *et al.*, Phys. Rev. D **92**, 052004 (2015).

[29] R. Agnese *et al.* (The SuperCDMS Collaboration), Phys. Rev. D **92**, 072003 (2015).

[30] C. Amole *et al.* (The PICO Collaboration), Phys. Rev. Lett. **114**, 231302 (2015).

[31] D. Y. Akimov *et al.*, Phys. Lett. B **709**, 14 (2012).

[32] P. Benetti *et al.* (The WArP Collaboration), Astropart. Phys. **28**, 495 (2008).